Chemical Physics Letters xxx (2017) xxx–xxx

Contents lists available at ScienceDirect

Chemical Physics Letters

journal homepage: www.elsevier.com/locate/cplett

Research paper

B_{26}^-: The smallest planar boron cluster with a hexagonal vacancy and a complicated potential landscape

Xue-Mei Luo [a], Tian Jian [b], Long-Jiu Cheng [c], Wan-Lu Li [d], Qiang Chen [a], Rui Li [a], Hua-Jin Zhai [a,e,*], Si-Dian Li [a,*], Alexander I. Boldyrev [c,*], Jun Li [c,*], Lai-Sheng Wang [b,*]

[a] Nanocluster Laboratory, Institute of Molecular Science, Shanxi University, Taiyuan 030006, China
[b] Department of Chemistry, Brown University, Providence, RI 02912, USA
[c] Department of Chemistry and Biochemistry, Utah State University, Logan, UT 84322-0300, USA
[d] Department of Chemistry & Key Laboratory of Organic Optoelectronics and Molecular Engineering of Ministry of Education, Tsinghua University, Beijing 100084, China
[e] State Key Laboratory of Quantum Optics and Quantum Optics Devices, Shanxi University, Taiyuan 030006, China

ARTICLE INFO

Article history:
Received 19 November 2016
In final form 22 December 2016
Available online xxxx

ABSTRACT

Anionic boron clusters have been systematically investigated both experimentally and theoretically up to 30 atoms and have all been proved to be planar or quasi-planar (2D) in their global minima. However, the B_{26}^- cluster has remained elusive in this size range up to now, because of its complicated potential landscape. Here we present a joint photoelectron spectroscopy (PES) and first-principles study on the structures and bonding of this seemingly enigmatic cluster. Extensive global minimum searches, followed by high-level calculations and Gibbs free energy corrections, reveal that at least three 2D isomers, **I** (C_1, ^{2}A), **II** (C_1, ^{2}A), and **III** (C_1, ^{2}A), could contribute to the observed PE spectrum for the B_{26}^- cluster. Isomer **I**, which has the lowest free energy at finite temperatures, is found to dominate the experimental spectrum and represents the smallest 2D boron cluster with a hexagonal vacancy. Distinct spectral features are observed for isomer **III**, which has a pentagonal hole and is found to contribute to the measured PE spectrum as a minor species. Isomer **II** with a close-packed triangular 2D structure, which is the global minimum at 0 K, may also contribute to the observed spectrum as a minor species. Chemical bonding analyses show that the principal isomer **I** can be viewed as an all-boron analog of the polycyclic aromatic hydrocarbon $C_{17}H_{11}^+$ in terms of the π bonds.

1. Introduction

As a result of its electron deficiency, boron has a strong propensity to form multicenter bonds in both of its bulk allotropes and its polyhedral compounds. Over the past two decades, extensive studies have been devoted to the investigations of the structures and bonding of size-selected boron clusters [1–10]. Multicenter bonding also appears to govern the unique planar or quasi-planar (2D) structures of a wide range of anionic boron clusters in the gas phase: B_n^- (n = 3–25, 27–30, 35, 36), whose global-minimum structures have been characterized in combined photoelectron spectroscopy (PES) and first-principles studies [10–27]. The 2D boron clusters all consist of B_3 triangles with tetragonal, pentagonal or hexagonal defects in some cases. The B_{27}^- cluster was recently shown to be the smallest 2D boron cluster to possess a coexisting isomer with a hexagonal vacancy along with a close-packed 2D global minimum with a tetragonal defect [21]. In all the 2D boron clusters, the periphery boron atoms form localized two-center two-electron (2c–2e) σ bonds, while the interior atoms are bonded via delocalized σ and π bonds, rendering aromaticity or antiaromaticity to the systems [9–29]. Notably, an analogy has been established in terms of π bonding between the 2D boron clusters and polycyclic aromatic hydrocarbons (PAHs), as exemplified by the B_{12}/benzene and B_{16}^{2-}/naphthalene analogy [12,13].

For larger boron clusters, a circular 2D B_{36} cluster with a central hexagonal hole, analogous to coronene ($C_{24}H_{12}$) [27], has been observed recently, which provides the first indirect evidence for the viability of 2D boron monolayers, named borophenes [26]. The B_{35}^- cluster with two adjacent hexagonal holes was found to be an even more flexible building block for borophenes [25]. More interestingly, a three-dimensional (3D) cage-like borospherene (D_{2d} $B_{40}^{-/0}$) analogous to fullerenes has been discovered [30], extending the analogy between boron and carbon. Subsequently, an axially chiral borospherene B_{39}^- and a seashell-like B_{28}^- cage have

* Corresponding authors at: Nanocluster Laboratory, Institute of Molecular Science, Shanxi University, Taiyuan 030006, China (H.-J. Zhai).
E-mail addresses: hj.zhai@sxu.edu.cn (H.-J. Zhai), lisidian@sxu.edu.cn (S.-D. Li), a.i.boldyrev@usu.edu (A.I. Boldyrev), junli@tsinghua.edu.cn (J. Li), lai-sheng_wang@brown.edu (L.-S. Wang).

http://dx.doi.org/10.1016/j.cplett.2016.12.051
0009-2614/

been reported [22,31], unveiling an interesting 2D–3D structural evolution in size-selected boron clusters. It should be noted that hexagonal holes are key structural features in both borophenes and borospherenes along with B_3 triangles.

Among the B_n^- clusters with n = 3–30, B_{26}^- has remained elusive experimentally to date, although there has been one theoretical report [32]. Hence, its true global minimum is still not known. We have found that the B_{26}^- cluster is quite challenging with a complicated potential landscape and several close-lying isomers, potentially contributing to the experiment. Hence, extreme care is required in the global minimum search, in conjunction with high-level *ab initio* calculations, in order to achieve satisfactory comparison with experiment.

In this article, we report the PE spectrum of B_{26}^- and extensive theoretical calculations to understand its structures and bonding. The current computational efforts include global minimum searches with several methods, PBE0 and coupled-cluster CCSD (T) calculations, and Gibbs free energy corrections at finite temperatures. We have found that two quasi-planar structures, **I** (C_1, ^{2}A) and **III** (C_1, ^{2}A), coexist in the B_{26}^- cluster beam, whereas another isomer **II** cannot be ruled out. Isomer **I** features a hexagonal hole at the center and is the major contributor to the observed PE spectrum, whereas isomer **III** with a pentagonal hole coexists as a minor species in the experiment. Isomer **II** with a closed-packed triangular lattice is found to be the global minimum at 0 K, similar to that reported previously [32]. However, isomer **I** becomes more stable at finite temperatures and is the smallest boron cluster to feature a hexagonal hole. Chemical bonding analyses show that isomer **I** is an all-boron analog of the PAH $C_{17}H_{11}^+$.

2. Experimental and theoretical methods

2.1. Photoelectron spectroscopy

The experiment was carried out using a magnetic-bottle PES apparatus, equipped with a laser vaporization cluster source [1,33]. The B_n^- cluster anions were produced from a disk target made of the ^{10}B isotope (98% enriched). Nascent clusters were entrained by a He carrier gas containing 5% Ar and underwent a supersonic expansion to form a collimated cluster beam. The cluster size distribution and cooling were controlled by the supersonic expansion, as well as the resident time of the clusters in the nozzle [1,34,35]. Anion clusters were extracted from the beam and analyzed using a time-of-flight mass spectrometer. The B_{26}^- cluster was mass-selected and decelerated before being intercepted by a detachment laser beam from an ArF excimer laser at 193 nm (6.424 eV). Photoelectrons were collected at nearly 100% efficiency and analyzed in a 3.5 m long electron flight tube. The PE spectrum was calibrated using the known spectrum of Au^-. The resolution of the apparatus was $\Delta E_k/E_k \approx 2.5\%$, that is, ~25 meV for 1 eV electrons. Although the actual temperature of the present B_{26}^- cluster beam was unknown in the experiment, our prior experience suggests that boron clusters in this size range should be at about room temperature or sub-room temperature [1,34,35].

2.2. Computational methods

Global minimum searches for B_{26}^- were performed at the density-functional theory (DFT) level using two independent methods: Minima Hopping (MH) [36] and Basin Hopping (BH) [37], in combination with manual structural constructions based on the known low-lying isomers of small boron clusters. The initial structures generated were optimized using the Perdew, Burke, and Ernzerhof exchange correlation functional (PBE0) [38] and the small 6-31G* basis set. Candidate low-lying isomers within 1.0 eV of the lowest energy structure were further refined using the PBE0 functional and the more expensive 6-311+G* basis set [39]. Frequency checks were performed at PBE0/6-311+G* to ensure that all reported isomers are true minima. Single-point CCSD(T)/6-311G* [40–42] calculations at the PBE0/6-311+G* geometries were further carried out for the top five lowest-lying isomers. Zero-point energy (ZPE) corrections were included in both the PBE0 and CCSD(T) calculations, at the PBE0/6-311+G* level.

Vertical detachment energies (VDEs) were calculated for the five lowest-lying isomers (**I**–**V**) at the PBE0/6-311+G* level. Higher VDEs were calculated at the time-dependent PBE0 (TD-PBE0) level [43]. Specifically, the ground-state VDE was calculated as the energy difference between the lowest anion state and the corresponding neutral state at the anion geometry, and the higher VDEs were obtained by adding the excitation energies of the corresponding electron transitions in the neutral to the ground-state VDE. PE spectra were simulated for isomers **I**–**V** by fitting the calculated VDEs with unit-area Gaussian functions of 0.05 eV half-width.

Chemical bonding analyses were performed using the adaptive natural density partitioning (AdNDP) method [44]. The AdNDP analyses were done at the PBE0 level and the results were visualized using Molekel 5.4.0.8 [45]. The PBE0 and TD-PBE0 calculations were performed using the Gaussian 09 program [46] and the single-point CCSD(T) calculations using the Molpro package [47]. Cluster structures and canonical molecular orbitals (CMOs) were visualized using GaussView 5.0.9 [48].

3. Results

3.1. Experimental results

The photoelectron spectrum of B_{26}^- at 193 nm is shown in Fig. 1a. Four main bands are observed (labeled as X, A, B, and C). Bands A and C are very broad and are likely to contain multiple detachment transitions. In addition, a weak band (X′) is observed at the low binding energy side and is likely from a minor isomer. The measured VDEs for these bands are given in Table 1, where they are compared with the calculated values.

Band X stands for the detachment transition from the ground state of the anion to that of the neutral, with a VDE of 3.99 eV measured from the peak maximum. The leading edge of the X band yields an estimated adiabatic detachment energy (ADE) of 3.82 eV, i.e. the electron affinity of the corresponding neutral cluster. The higher binding energy peaks (A, B, and C) correspond to detachment transitions from the anion ground state to the low-lying excited states of the neutral. Band A covers an energy range from ~4.2 to ~5.1 eV, centering at ~4.6 eV. The next band B with a VDE of 5.35 eV is relatively sharp. Beyond ~5.5 eV the electron signals are continuous with poor signal-to-noise ratios, and a band C at ~6 eV is tentatively labeled for the sake of discussion. The weak band X′ at the low binding energy side yields a VDE and ADE of 3.65 and 3.55 eV, respectively, for the possible minor isomer.

3.2. Global minimum searches and low-lying isomers of B_{26}^-

We generated over 6500 stationary points on the potential energy surface of the B_{26}^- cluster, using the MH and BH algorithms along with manual structure constructions. Low-lying structures were then reoptimized and their relative energies evaluated at the PBE0/6-311+G* level. We identified about 80 structures within 1.0 eV at the PBE0 level, as shown in the supplementary material (Fig. S1). The top five isomers of B_{26}^- are within ~0.5 eV at PBE0, as illustrated in Fig. 2a. Cartesian coordinates of these isomers are given in the supplementary material (Table S2). Four of the

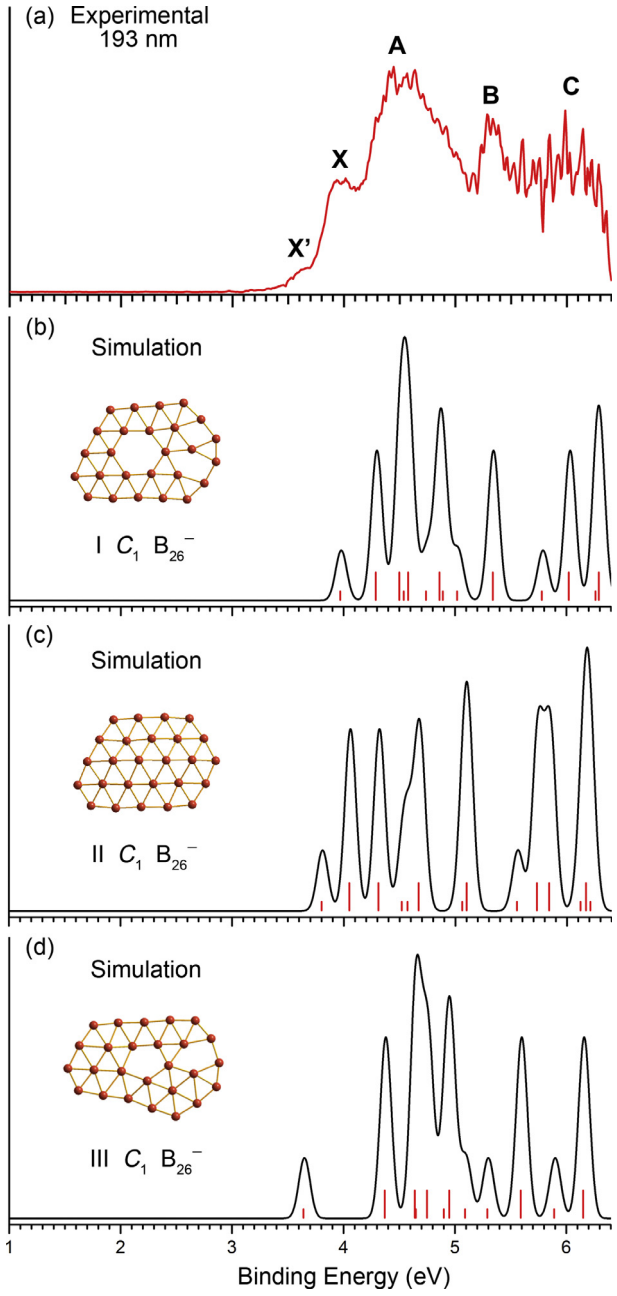

Fig. 1. Photoelectron spectrum of the B_{26}^- cluster at 193 nm (6.424 eV) (a) and comparison with the simulated spectra at the PBE0/6-311+G* level for isomers **I** (b), **II** (c), and **III** (d). The simulated spectra were obtained by fitting the calculated vertical detachment energies (VDEs) with unit-area Gaussian functions of 0.05 eV half-width. Vertical bars in (b), (c), and (d) represent the calculated VDEs, and an intensity ratio of 3 to 1 is assumed in the fitting for triplet versus singlet final states.

low-lying structures are 2D (**I**–**III** and **V**), and the close-packed triangular isomer **II** is the lowest in energy at PBE0. The double-ring tubular isomer **IV** is virtually isoenergetic to isomer **II** (within 0.01 eV) at this level of theory. We recalculated the top five isomers at the CCSD(T)/6-311G* level using the PBE0 geometries, and found that the energy order altered. Isomer **II** remains the lowest in energy, but isomer **I** is much stabilized, becoming only 0.15 eV higher and almost degenerate with the double-ring isomer **IV** (Fig. 2a). The isomers **II**, **IV**, and **V** were also considered in a previous theoretical study [32], which suggested that the double-ring isomer **IV** was the global minimum, followed by isomer **II**.

We found that the potential landscape of the neutral B_{26} cluster is quite different from that of the anion. The five low-lying neutral structures (**VI**–**X**) are shown in Fig. 2b at the PBE0 level. The tubular isomer **VI** is the lowest in energy, followed by the close-packed triangular 2D isomer **VII**. These two structures are related to the anion isomers **IV** and **II**, respectively. The next three neutral isomers (**VIII**–**X**) are all 3D cage-like, but they are at least ~0.5 eV above the global minimum.

3.3. Gibbs free energy corrections

We found initially that the simulated PE spectrum of the global minimum isomer **II** did not agree well with the experimental PES data (*vide infra*), which had puzzled us for quite a long time and was the main reason keeping us from solving the structure of B_{26}^-. To resolve the disagreement between theory and experiment, we considered the Gibbs free energy corrections beyond the single-point CCSD(T) energetics for the top five isomers, by taking into account the entropic effects at finite temperatures. Fig. 3 shows the dependence of the relative energies of the top five isomers (**I**–**V**) as a function of temperature from 0 to 600 K, using isomer **II** as a reference. We found that the stabilities of isomers **IV** and **V** with respect to **II** remain roughly constant in this temperature range. However, isomers **I** and **III** become much more stable at elevated temperatures. Above ~440 K, isomer **I** becomes more stable than isomer **II** (Fig. 3). The relative energies with Gibbs free energy corrections at 460 K for isomers **I** to **V** of B_{26}^- are also given in Fig. 2a. At this temperature, isomers **I** and **II** are almost degenerate, with isomer **III** only 0.11 eV higher and isomer **IV** 0.13 eV higher. Even though our previous experiences suggested that clusters from our laser vaporization supersonic source should be at room temperature or sub-room temperature [1,34,35], the dependence of the relative stabilities of the different isomers of B_{26}^- indicated that we needed to consider at least the top four isomers in the comparison with the experiment, considering the accuracy of the theoretical calculations.

4. Discussion

4.1. Comparison between experiment and theory and the structural plurality of B_{26}^-

Since all the low-lying isomers of B_{26}^- are open-shell with an unpaired electron (Fig. 2a), both singlet and triplet final states will be resulted upon electron detachment. The calculated VDEs and simulated PE spectra for isomers **I**, **II**, and **III** are compared with the experimental data in Fig. 1 and Table 1 (complete VDEs for isomers **II** and **III** are given in Table S1). The simulated spectra for isomers **IV** and **V** are compared with the experiment in Fig. S2. The double-ring isomer **IV** with high symmetry yielded a relatively simple simulated spectrum (Fig. S2b), which completely disagreed with the experimental data. Isomer **V** can also be ruled out on the bases of both its energetics and its simulated PE spectrum (Fig. S2c).

The calculated first VDE/ADE for isomer **I** are 3.97/3.76 eV, in excellent agreement with the experimental measurements of 3.99/3.82 eV from band X. The computed higher VDEs for isomer **I** are also in good accord with the experimental data. In particular, as many as eight detachment channels are predicted between 4.3 and 5.0 eV, corresponding to the broad A band. The overall spectral pattern of the simulated spectrum for isomer **I** (Fig. 1b) agrees well with the experimental spectrum, lending considerable credence to the assignment of isomer **I** as the main carrier of the PE spectrum. This conclusion is consistent with the fact that isomer **I** becomes more stable at finite temperatures.

Table 1
Experimental vertical detachment energies (VDE in eV) of B_{26}^- compared with those calculated at the PBE0/6-311+G* and time-dependent PBE0/6-311+G* (TD-PBE0) levels for isomers **I** and **III**.

Feature	VDE (exp)[a]	Final state	Electronic configuration	VDE (TD-PBE0)[b]
			Isomer **I** (C_1, ^{2}A)	
X[c]	3.99 (5)	^{1}A	$(32a)^2(33a)^2(34a)^2(35a)^2(36a)^2(37a)^2(38a)^2(39a)^2(40a)^0$	3.97
A	~4.6	^{3}A	$(32a)^2(33a)^2(34a)^2(35a)^2(36a)^2(37a)^2(38a)^2(39a)^1(40a)^1$	4.29
		^{3}A	$(32a)^2(33a)^2(34a)^2(35a)^2(36a)^2(37a)^2(38a)^1(39a)^2(40a)^1$	4.50
		^{1}A	$(32a)^2(33a)^2(34a)^2(35a)^2(36a)^2(37a)^2(38a)^2(39a)^1(40a)^1$	4.54
		^{3}A	$(32a)^2(33a)^2(34a)^2(35a)^2(36a)^2(37a)^1(38a)^2(39a)^2(40a)^1$	4.58
		^{1}A	$(32a)^2(33a)^2(34a)^2(35a)^2(36a)^2(37a)^2(38a)^1(39a)^2(40a)^1$	4.74
		^{3}A	$(32a)^2(33a)^2(34a)^2(35a)^2(36a)^1(37a)^2(38a)^2(39a)^2(40a)^1$	4.86
		^{1}A	$(32a)^2(33a)^2(34a)^2(35a)^2(36a)^2(37a)^1(38a)^2(39a)^2(40a)^1$	4.89
		^{1}A	$(32a)^2(33a)^2(34a)^2(35a)^2(36a)^1(37a)^2(38a)^2(39a)^2(40a)^1$	5.02
B	5.35 (5)	^{3}A	$(32a)^2(33a)^2(34a)^2(35a)^1(36a)^2(37a)^2(38a)^2(39a)^2(40a)^1$	5.34
C	~6.1	^{1}A	$(32a)^2(33a)^2(34a)^2(35a)^1(36a)^2(37a)^2(38a)^2(39a)^2(40a)^1$	5.78
		^{3}A	$(32a)^2(33a)^2(34a)^1(35a)^2(36a)^2(37a)^2(38a)^2(39a)^2(40a)^1$	6.02
		^{1}A	$(32a)^2(33a)^2(34a)^1(35a)^2(36a)^2(37a)^2(38a)^2(39a)^2(40a)^1$	6.26
		^{3}A	$(32a)^2(33a)^1(34a)^2(35a)^2(36a)^2(37a)^2(38a)^2(39a)^2(40a)^1$	6.29
			Isomer **III** (C_1, ^{2}A)	
X'[d]	3.65 (5)	^{1}A	$(32a)^2(33a)^2(34a)^2(35a)^2(36a)^2(37a)^2(38a)^2(39a)^2(40a)^0$	3.64

[a] The number in the parenthesis represents the uncertainty in the last digit.
[b] Ground-state VDEs were calculated at PBE0/6-311+G* level and higher VDEs at TD-PBE0/6-311+G*.
[c] The ADE for band X was measured to be 3.82 (5) eV.
[d] The ADE for band X' was measured to be 3.55 (5) eV.

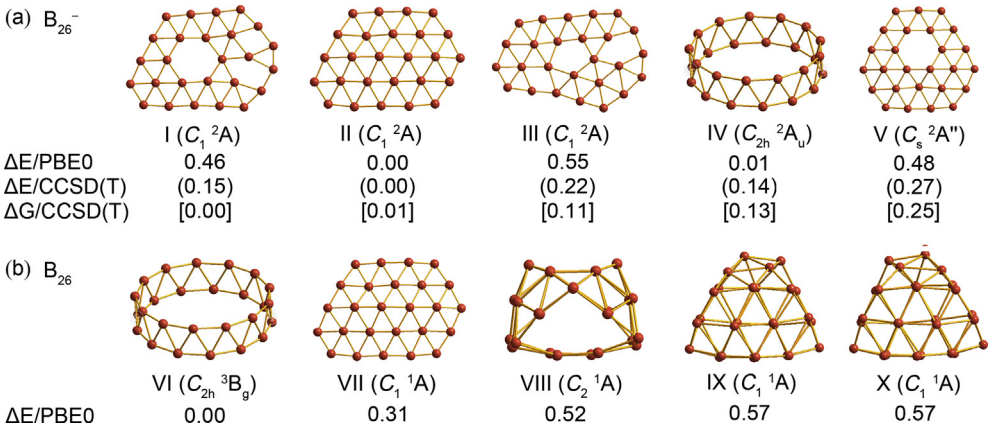

Fig. 2. The top low-lying isomers of B_{26}^- (a). Relative energies are shown in eV at the PBE0/6-311+G*, CCSD(T)/6-311 G*//PBE0/6-311+G* (in parenthesis), and CCSD(T)/6-311 G*//PBE0/6-311+G* with corrections for Gibbs free energy at 460 K (in square brackets) levels. The PBE0 and CCSD(T) data are corrected for zero-point energies at the PBE0/6-311+G* level. Gibbs free energies are calculated using the CCSD(T) energies with corrections for entropic effects at the PBE0/6-311+G* level. The top Low-lying isomers for B_{26} neutral at the PBE0 level are also shown (b).

The first calculated VDE for isomer **III** is 3.64 eV, in excellent agreement with the measured VDE of 3.65 eV for the weak X′ band (Table 1). The calculated higher VDEs for isomer **III** are likely buried in the strong signals of isomer **I.** From the energetic point of view, isomer **II** should also be present in the experiment. However, its simulated spectrum (Fig. 1c) does not agree with the experiment as well as that of isomer **I**, and hence it could not be the major contributor to the observed spectrum. Nevertheless, its calculated spectral features are all in the same energy range as those of isomer **I** and could be buried under the dominating detachment transitions of isomer **I**. Therefore, we conclude that all three isomers were present in the cluster beam with isomer **I** as the major species and the most important isomer under our experimental conditions.

The presence of close-lying isomers has also been observed for other boron clusters, for example, for both B_{40}^- and B_{39}^- [30,31] and most recently for B_{29}^- [23]. This tends to occur when clusters undergo major structural changes (for instance, from close-packed planar, to planar with hexagonal defects, to multi-ring tubular, or even to cage-like structures). In such cases, different structural types compete, posing significant experimental and computational challenges. In the current case, isomers **I**, **II**, and **III** of the B_{26}^- cluster each represent a distinct 2D structural type and B_{26}^- is the onset of 2D boron clusters with hexagonal defects within the triangular lattice. The hexagonal vacancy is a major structural feature of 2D borons, as first discovered in B_{36}^- [26], which led to the proposal of the concept of borophenes and provided the first indirect experimental evidence for the viability of this new 2D material [49,50].

*4.2. Chemical bonding in isomer **I** of B_{26}^-: The smallest boron cluster with a hexagonal hole*

High-lying isomers with a hexagonal hole have been observed in smaller boron clusters [17–20]. A low-lying isomer with a hexagonal hole has been observed experimentally for B_{27}^- [21]. B_{26}^- is the smallest cluster, which has an isomer with a hexagonal hole competing for the global minimum and is the major species observed

experimentally. We have analyzed the nature of the chemical bonding in the dominating isomer **I** using both CMOs and AdNDP. Since isomer **I** is quasi-planar and open-shell, we chose to use the corresponding flattened, closed-shell B_{26}^{2-} version for the convenience of bonding analyses. We found that B_{26}^{2-} possesses eight delocalized π CMOs, exhibiting a one-to-one correspondence to the π CMOs of the PAH $C_{17}H_{11}^{+}$ (C_s, $^1A'$) (Fig. 4). Hence, isomer **I** of B_{26}^{-} can be viewed as an all-boron analog of $C_{17}H_{11}^{+}$, continuing the hydrocarbon analogy of 2D boron clusters.

Fig. 5 compares the AdNDP results between B_{26}^{2-} and $C_{17}H_{11}^{+}$. Among the 40 electron pairs in B_{26}^{2-}, sixteen are localized as periphery 2c-2e σ bonds with occupation numbers (ONs) between

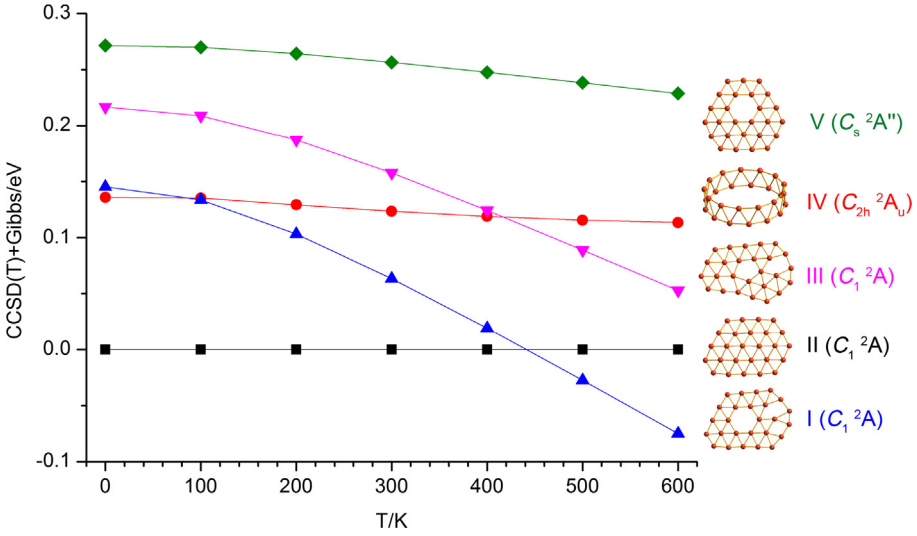

Fig. 3. Gibbs free energies of the top five low-lying isomers of B_{26}^{-} cluster as a function of temperature (from 0 to 600 K). The energies are at the single-point CCSD(T) level with Gibbs free energy corrections at PBE0/6-311+G*, plotted relative to that of isomer **II**.

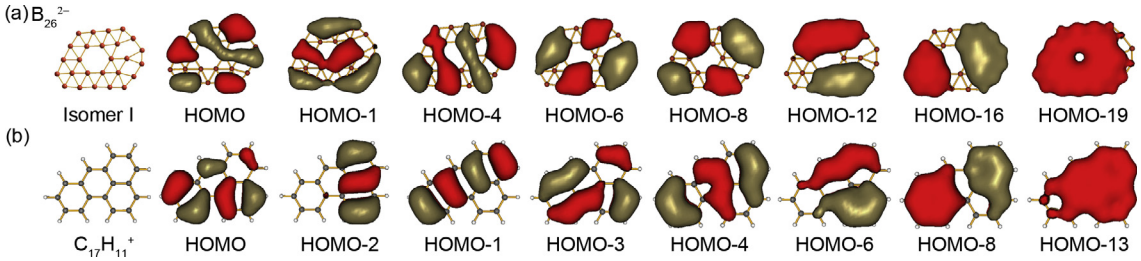

Fig. 4. Comparison of the canonical π molecular orbitals of the closed-shell B_{26}^{2-} (a) and the polycyclic aromatic hydrocarbon $C_{17}H_{11}^{+}$ (b). The closed-shell B_{26}^{2-} species is formed by adding an electron to a flattened version of isomer **I** of B_{26}^{-} for the convenience of analyses and presentation.

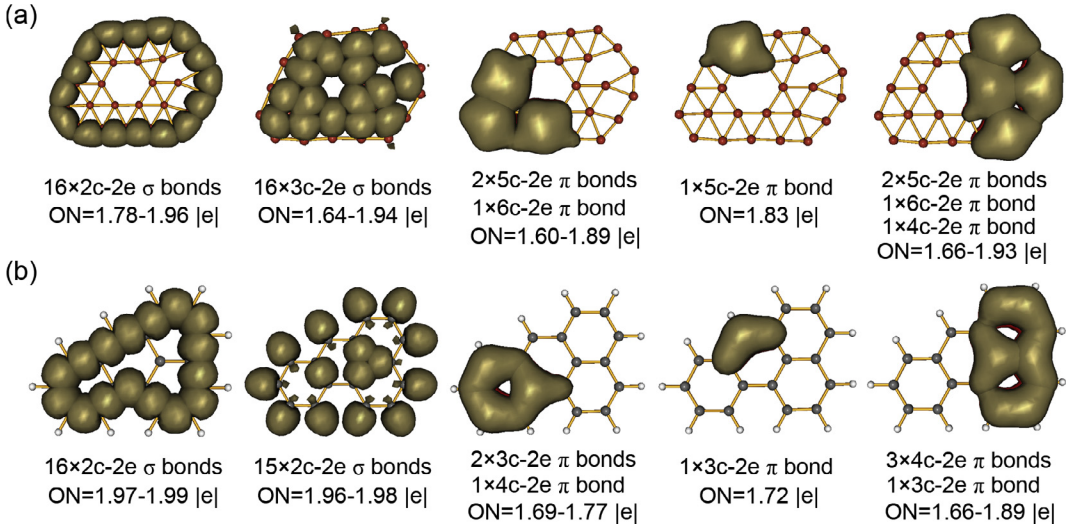

Fig. 5. Comparison of the AdNDP analyses for B_{26}^{2-} corresponding to isomer **I** of B_{26}^{-} (a) and the polycyclic aromatic hydrocarbon $C_{17}H_{11}^{+}$ (b). The occupation numbers (ONs) are shown.

Please cite this article in press as: X.-M. Luo et al., Chem. Phys. Lett. (2017), http://dx.doi.org/10.1016/j.cplett.2016.12.051

1.78–1.96 |e| (Fig. 5a). The ten interior B atoms are bonded with each other and with the peripheral B atoms by sixteen delocalized 3c–2e σ bonds with ONs of 1.64–1.94 |e|. The remaining eight electron pairs involve multi-center delocalized π bonding. The distribution of the eight π bonds in B_{26}^{2-} is almost exactly the same as that in $C_{17}H_{11}^{+}$ (Fig 5b), further supporting the PAH analogy of 2D boron clusters.

5. Conclusions

We report a joint PES and theoretical study on the structures and bonding of the elusive B_{26}^{-} cluster. Extensive global minimum searches in conjunction with high-level *ab initio* calculations revealed that there are three close-lying isomers, which contributed to the experimental spectrum. Isomer **I** represents the smallest 2D boron cluster with a hexagonal vacancy and isomer **II** corresponds to a close-packed triangular structure, whereas isomer **III** contains a pentagonal defect. At 0 K, isomer **II** is the global minimum, but both isomers **I** and **III** become more stable at finite temperatures. Isomer **I** is found to be the main carrier of the observed PE spectrum, while distinct PES features are also observed for the isomer **III**. The current study reveals a complicated potential landscape for B_{26}^{-}, which is the onset for the structural transition evolution of boron clusters from pentagonal vacancy to hexagonal vacancy. The latter is prevalent in larger boron clusters and is a key structural feature of borophenes.

Acknowledgments

The experimental work done at Brown University was supported by the US National Science Foundation (CHE-1632813 to L.S.W.). The theoretical work was supported by the National Natural Science Foundation of China (21573138, 21373130, 21521091) and the State Key Laboratory of Quantum Optics and Quantum Optics Devices (KF201402), and the US National Science Foundation (CHE-1361413 to A.I.B.).

Appendix A. Supplementary material

Supplementary data associated with this article can be found, in the online version, at http://dx.doi.org/10.1016/j.cplett.2016.12.051.

References

[1] L.S. Wang, Int. Rev. Phys. Chem. 35 (2016) 69.
[2] E. Oger, N.R.M. Crawford, R. Kelting, P. Weis, M.M. Kappes, R. Ahlrichs, Angew. Chem. Int. Ed. 46 (2007) 8503.
[3] A.P. Sergeeva, I.A. Popov, Z.A. Piazza, W.L. Li, C. Romanescu, L.S. Wang, A.I. Boldyrev, Acc. Chem. Res. 47 (2014) 1349.
[4] A.N. Alexandrova, A.I. Boldyrev, H.J. Zhai, L.S. Wang, Coord. Chem. Rev. 250 (2006) 2811.
[5] L. Hanley, J.L. Whitten, S.L. Anderson, J. Phys. Chem. 92 (1988) 5803.
[6] R. Kawai, J.H. Weare, J. Chem. Phys. 95 (1991) 1151.
[7] I. Boustani, Phys. Rev. B 55 (1997) 16426.
[8] A. Ricca, C.W. Bauschlicher Jr, Chem. Phys. Lett. 208 (1996) 233.
[9] J.E. Fowler, J.M. Ugalde, J. Phys. Chem. A 104 (2000) 397.
[10] H.J. Zhai, L.S. Wang, A.N. Alexandrova, A.I. Boldyrev, J. Chem. Phys. 117 (2002) 7917.
[11] H.J. Zhai, A.N. Alexandrova, K.A. Birch, A.I. Boldyrev, L.S. Wang, Angew. Chem. Int. Ed. 42 (2003) 6004.
[12] H.J. Zhai, B. Kiran, J. Li, L.S. Wang, Nat. Mater. 2 (2003) 827.
[13] A.P. Sergeeva, D.Y. Zubarev, H.J. Zhai, A.I. Boldyrev, L.S. Wang, J. Am. Chem. Soc. 130 (2008) 7244.
[14] A.P. Sergeeva, B.B. Averkiev, H.J. Zhai, A.I. Boldyrev, L.S. Wang, J. Chem. Phys. 134 (2011) 224304.
[15] W. Huang, A.P. Sergeeva, H.J. Zhai, B.B. Averkiev, L.S. Wang, A.I. Boldyrev, Nat. Chem. 2 (2010) 202.
[16] B. Kiran, S. Bulusu, H.J. Zhai, S. Yoo, X.C. Zeng, L.S. Wang, Proc. Natl. Acad. Sci. U. S. A. 102 (2005) 961.
[17] Z.A. Piazza, W.L. Li, C. Romanescu, A.P. Sergeeva, L.S. Wang, A.I. Boldyrev, J. Chem. Phys. 136 (2012) 104310.
[18] A.P. Sergeeva, Z.A. Piazza, C. Romanescu, W.L. Li, A.I. Boldyrev, L.S. Wang, J. Am. Chem. Soc. 134 (2012) 18065.
[19] I.A. Popov, Z.A. Piazza, W.L. Li, L.S. Wang, A.I. Boldyrev, J. Chem. Phys. 139 (2013) 144307.
[20] Z.A. Piazza, I.A. Popov, W.L. Li, R. Pal, X.C. Zeng, A.I. Boldyrev, L.S. Wang, J. Chem. Phys. 141 (2014) 034303.
[21] W.L. Li, R. Pal, Z.A. Piazza, X.C. Zeng, L.S. Wang, J. Chem. Phys. 142 (2015) 204305.
[22] Y.J. Wang, Y.F. Zhao, W.L. Li, T. Jian, Q. Chen, X.R. You, T. Ou, X.Y. Zhao, H.J. Zhai, S.D. Li, J. Li, L.S. Wang, J. Chem. Phys. 144 (2016) 064307.
[23] H.R. Li, T. Jian, W.L. Li, C.Q. Miao, Y.J. Wang, Q. Chen, X.M. Luo, K. Wang, H.J. Zhai, S.D. Li, L.S. Wang, Phys. Chem. Chem. Phys. 18 (2016) 29147.
[24] W.L. Li, Y.F. Zhao, H.S. Hu, J. Li, L.S. Wang, Angew. Chem. Int. Ed. 53 (2014) 5540.
[25] W.L. Li, Q. Chen, W.J. Tian, H. Bai, Y.F. Zhao, H.S. Hu, J. Li, H.J. Zhai, S.D. Li, L.S. Wang, J. Am. Chem. Soc. 136 (2014) 12257.
[26] Z.A. Piazza, H.S. Hu, W.L. Li, Y.F. Zhao, J. Li, L.S. Wang, Nat. Commun. 5 (2014) 3113.
[27] Q. Chen, G.F. Wei, W.J. Tian, H. Bai, Z.P. Liu, H.J. Zhai, S.D. Li, Phys. Chem. Chem. Phys. 16 (2014) 18282.
[28] D.Y. Zubarev, A.I. Boldyrev, J. Comput. Chem. 28 (2007) 251.
[29] A.I. Boldyrev, L.S. Wang, Phys. Chem. Chem. Phys. 18 (2016) 11589.
[30] H.J. Zhai, Y.F. Zhao, W.L. Li, Q. Chen, H. Bai, H.S. Hu, Z.A. Piazza, W.J. Tian, H.G. Lu, Y.B. Wu, Y.W. Mu, G.F. Wei, Z.P. Liu, J. Li, S.D. Li, L.S. Wang, Nat. Chem. 6 (2014) 727.
[31] Q. Chen, W.L. Li, Y.F. Zhao, S.Y. Zhang, H.S. Hu, H. Bai, H.R. Li, W.J. Tian, H.G. Lu, H.J. Zhai, S.D. Li, J. Li, L.S. Wang, ACS Nano 9 (2015) 754.
[32] T.B. Tai, M.T. Nguyen, Phys. Chem. Chem. Phys. 17 (2015) 13672.
[33] L.S. Wang, H.S. Cheng, J.W. Fan, J. Chem. Phys. 102 (1995) 9480.
[34] J. Akola, M. Manninen, H. Hakkinen, U. Landman, X. Li, L.S. Wang, Phys. Rev. B 60 (1999) R11297.
[35] W. Huang, L.S. Wang, Phys. Rev. Lett. 102 (2009) 153401.
[36] S. Goedecker, J. Chem. Phys. 120 (2004) 9911.
[37] D.J. Wales, H.A. Scheraga, Science 285 (1999) 1368.
[38] C. Adamo, V. Barone, J. Chem. Phys. 110 (1999) 6158.
[39] R. Krishnan, J.S. Binkley, R. Seeger, J.A. Pople, J. Chem. Phys. 72 (1980) 650.
[40] J. Čížek, Adv. Chem. Phys. 14 (1969) 35.
[41] G.D. Purvis III, R.J. Bartlett, J. Chem. Phys. 76 (1982) 1910.
[42] K. Raghavachari, G.W. Trucks, J.A. Pople, M. Head-Gordon, Chem. Phys. Lett. 157 (1989) 479.
[43] R. Bauernschmitt, R. Ahlrichs, Chem. Phys. Lett. 256 (1996) 454.
[44] D.Y. Zubarev, A.I. Boldyrev, Phys. Chem. Chem. Phys. 10 (2008) 5207.
[45] U. Varetto, Molekel 5.4.0.8, Swiss National Supercomputing Center, Manno, Switzerland, 2009.
[46] M.J. Frisch et al., Gaussian 09, Revision D.01, Gaussian Inc, Wallingford, CT, 2009.
[47] H.J. Werner, P.J. Knowles, G. Knizia, F.R. Manby, M. Schütz, P. Celani, T. Korona, R. Lindh, A. Mitrushenkov, G. Rauhut, et al., MOLPRO, version 2012.1, A package of ab initio programs, 2012; see <http://www.molpro.net>.
[48] R. Dennington, T. Keith, J. Millam, GaussView, version 5.0.9, Semichem Inc, Shawnee Mission, KS, 2009.
[49] A.J. Mannix, X.F. Zhou, B. Kiraly, J.D. Wood, D. Alducin, B.D. Myers, X.L. Liu, B.L. Fisher, U. Santiago, J.R. Guest, M.J. Yacaman, A. Ponce, A.R. Oganov, M.C. Hersam, N.P. Guisinger, Science 350 (2015) 1513.
[50] B.J. Feng, J. Zhang, Q. Zhong, W.B. Li, S. Li, H. Li, P. Cheng, S. Meng, L. Chen, K.H. Wu, Nat. Chem. 8 (2016) 563.